to appear in THE ASTROPHYSICAL JOURNAL

THE INHOMOGENEOUS JET PARAMETERS IN ACTIVE GALACTIC NUCLEI

D. R. JIANG, XINWU CAO, AND XIAOYU HONG
Shanghai Observatory, Chinese Academy of Sciences, Shanghai, 200030, China;
djiang@center.shao.ac.cn

ABSTRACT

The Königl inhomogeneous jet model is applied to investigate the properties of the jets in Active Galactic Nuclei (AGNs). A sample of the AGNs is collected, in which the measurements of the angular size and radio flux density of the VLBI core, proper motion of the components in the jet, and X-ray flux density are included. The inhomogeneous jet parameters are derived with the same assumptions for all sources. A comparison among the parameters of different types of sources in the sample is presented. It is found that most of EGRET (Energetic Gamma-ray Experiment Telescope) sources have higher Doppler factor δ, larger Lorentz factor γ, and smaller viewing angle θ, when compared with the remaining sources in the sample. The statistical analyses show that the derived Doppler factor δ is strongly correlated with the observed 22 GHz brightness temperature. Furthermore, there is a correlation between the relative γ-ray luminosity and the Doppler factor δ. The implications of these results are discussed.

Subject headings: galaxies: kinematics and dynamics — galaxies: nuclei, jets.

1. INTRODUCTION

Superluminal motion has been observed in many active galactic nuclei (AGN) with VLBI. This provides strong evidence that the plasma in the jets moves at relativistic velocity. In the framework of the unified scheme, the different classes of AGNs (such as radio galaxies, radio-loud quasars, and blazars) can be interpreted as the same kind of sources but viewed at different directions. Therefore the bulk velocity in the jets and the viewing angles are two key parameters for our understanding the physics of jets and discriminating models of AGNs.

The energetic γ-ray emissions from the AGNs offers an important clue to understand the physics at work in the AGNs. Only one quasar (3C273) had been detected in high energy γ-ray emission before the launch of the Energetic Gamma-Ray Experiment Telescope (EGRET) on

board the Compton Gamma-Ray Observatory. So far, the EGRET has detected about 50 AGN (von Montigny et al., 1995; Thompson et al. 1995). Some interesting results from the observations are summarized as follows (von Montigny et al., 1995): (1) The γ-ray energy flux in many of the sources is dominant over the flux at lower energy bands. The typical isotropic apparent γ-ray luminosities are in the range of $10^{45} - 10^{49}$ ergs s^{-1} . (2) Many of the sources exhibit rapid variability on time scales from days to months, which implies that the size of emitting region is of the order of the Schwarzschild radius of a black hole with 10^{10} $M_\odot$ under isotropic emission assumption. (3) Many active galaxies relatively close to the Earth and some of the superluminal radio sources have not been detected.

The proper motion measurements in the compact structures of the AGNs provide useful information on the bulk motions of the emitting plasma. In the framework of the relativistic beaming model and the synchrotron self-Compton (SSC) model, the VLBI observations combined with the X-ray flux density could be used to derive the Doppler boosting factor and some physical quantities in the emitting regions of the AGNs. Marscher (1987) derived the beaming parameters on the assumption of homogeneous spherical emission plasma. Ghisellini et al. (1993) adopted Marscher's approach and obtained the Doppler boosting factor δ for 105 sources. Readhead (1994) suggested to estimate the value of equipartition Doppler boosting factor δ_{eq} using a single epoch radio data by assuming that the sources are to in equipartition between the energy of radiating particles and the magnetic field. Güijosa and Daly (1996) derived the δ_{eq} for the same sample in Ghisellini et al. (1993). The advantage of homogeneous sphere model is that the formalism is simple and the value of δ derived is independent on the cosmology model. The component angular size and the flux at the turnover frequency should be known in their calculation. In practice, it is difficult to obtain this information, so one has to assume that the VLBI observing frequency is the synchrotron self-absorption frequency. In addition, the dependence of core size on the observing frequency in some sources is inconsistent with the homogeneous spherical assumption.

Blandford and Königl (1979) and Königl (1981) presented an inhomogeneous relativistic jet model, in which both the flat spectrum characteristics of some AGNs and the dependence of the core size on the observing frequency could be well explained. Königl's model involves more free parameters than the homogeneous model, which limits its application. Some authors (Hutter and Mufson 1986; Mufson et al, 1989; Unwin et al. 1994; Zensus et al. 1989 & Webb et al. 1994) have explored the application of this kind of model to obtain some physical parameters in some sources.

We assemble an AGN sample with both VLBI and X-ray observations available. Königl's inhomogeneous jet model is applied in our work to derive the physical parameters of the jets. In § 2 we briefly describe the jet model formalism and the approach. The sample and the results are described in § 3 and § 4, respectively. The § 5 contains a short discussion.

2. MODEL

Königl (1981) proposed an inhomogeneous jet model, in which the magnetic field B(r) and the number density of the relativistic electrons $n_e(r, \gamma_e)$ in the jet are assumed to vary with the distance from the apex of the jet r as $B(r) = B_1(r/r_1)^{-m}$ and $n_e(r, \gamma_e) = n_1(r/r_1)^{-n}{\gamma_e}^{-(2\alpha+1)}$ respectively, and $r_1 = 1pc$. If the bulk motion velocity of the jet is βc (corresponding to a Lorentz factor γ) with an opening half-angle ϕ, and the axis of the jet makes an angle θ with the direction of the observer, the distance from the origin of the jet, $r(\tau_{\nu_s} = 1)$, at which the optical depth to the synchrotron self-absorption at the observing frequency ν_s equals unity, is given by equation (3) in Königl (1981) as

$$\frac{r(\tau_{\nu_s} = 1)}{r_1} = (2c_2(\alpha)r_1 n_1 \phi \csc\theta)^{2/(2\alpha+5)k_m} (B_1\delta)^{(2\alpha+3)/(2\alpha+5)k_m} (\nu_s(1+z))^{-1/k_m}. \quad (1)$$

Here $c_2(\alpha)$ is the constant in the synchrotron absorption coefficient, δ is the Doppler factor, and $k_m = [2n + m(2\alpha + 3) - 2]/(2\alpha + 5)$. We use the projection of the optically thick region in the jet as a measurement of the observed VLBI core angular size θ_d,

$$\theta_d = \frac{r(\tau_{\nu_s} = 1)\sin\theta}{D_a}, \quad (2)$$

where D_a is the angular diameter distance of the source.

By integration of the emission from the optically thick region along the jet, we obtain the radio flux of the core as

$$s(\nu_s) = \frac{1}{4\pi D_a^2}\frac{c_1(\alpha)}{c_2(\alpha)} B_1^{-1/2} \left(\frac{\delta}{1+z}\right)^3 \left[\frac{\nu_s(1+z)}{\delta}\right]^{5/2} \int_0^{r(\tau_{\nu_s}=1)} 2\left(\frac{r}{r_1}\right)^{m/2} \varphi r \sin\theta dr$$

$$= \frac{r_1^2 \phi \sin\theta}{(4+m)\pi D_a^2}\frac{c_1(\alpha)}{c_2(\alpha)} B_1^{-1/2} \nu_s^{5/2} \left(\frac{\delta}{1+z}\right)^{1/2} \left(\frac{r(\tau_{\nu_s}=1)}{r_1}\right)^{(4+m)/2}, \quad (3)$$

where ν_s is the VLBI observing frequency, and $c_1(\alpha)$ and $c_2(\alpha)$ are the constants in the synchrotron emission and absorption coefficients, respectively.

Equation (13) in Königl's work gives the X-ray flux density estimation from an unresolved jet. We adopt his expression in the frequency region $\nu_c > \nu_{cb}(r_M)$, where r_M is the smallest radius from which optically thin synchrotron emission with spectral index α is observed (Königl 1981).

The proper motion observed with VLBI could be converted to the apparent transverse velocity β_{app} by using the Friedmann cosmology. The apparent transverse velocity β_{app} is related to the bulk velocity of the jet βc and viewing angle θ,

$$\beta_{app} = \frac{\beta\sin\theta}{1 - \beta\cos\theta}, \quad (4)$$

if the viewing angle θ is available.

The above equations, in conjunction with equation (13) in Königl(1981), can well describe the relation between the physical parameters of the inhomogeneous relativistic jet model and the observational results. The parameters of an inhomogeneous jet could be derived from both VLBI and X-ray observations given the three parameters α, m, n, and the relation between the opening half angle ϕ and the Lorentz factor γ. Three parameters α, m and n are related to α_{S1}, α_{C2} and k_m as following:

$$\alpha_{S1} = \frac{5}{2} - \frac{4+m}{2k_m}, \tag{5}$$

$$\alpha_{C2} = \alpha + \frac{(1+\alpha)m + 2n - 4}{7m - 4} \tag{6}$$

and

$$k_m = \frac{2n + m(2\alpha + 3) - 2}{2\alpha + 5}, \tag{7}$$

where α_{S1} is the spectral index of the VLBI core at radio band, α_{C2} is the spectral index at X-ray band ($S_\nu \propto \nu^{-\alpha}$) and k_m relates the dependence of the core angular size on the observing frequency ($\theta_d \propto \nu_{ob}^{-1/k_m}$).

In principle, three parameters α, m and n could be constrained by the observable quantities α_{S1}, α_{C2} and k_m. Many workers have tried to explore the mean value of the spectral index. Padovani et al. (1997) suggested that the mean value of the spectral index in the X-ray band of the flat-spectrum radio quasars is $\langle\alpha_x\rangle \sim 1$. Brunner et al. (1994) obtained $\langle\alpha_x\rangle \sim 0.6$ for radio loud quasars. Lamer et al. (1996) found $\langle\alpha_x\rangle \sim 1.30$ for BL Lac objects. Padovani and Urry (1992) used $\langle\alpha_{S1}\rangle \sim -0.1$ for flat spectrum radio quasars. For BL Lac objects, $\langle\alpha_{S1}\rangle \sim -0.3$ is given by Padovani (1992). In the cases where there are multi-frequency VLBI observations, $k_m \sim 1$ is found.

Unwin et al.(1994) found $\alpha = 0.6$, $m = 1.5$ and $n = 1.4$ for the conical jet model in 3C345. The values of k_m, α_{S1} and α_{C2} in that case are 1.145, -0.1 and 0.78, respectively. These values agree with the statistical values. Hutter and Mufson (1986) expected $m = 1$ and $n = 2$ for a free jet. Webb et al. (1994) derived $m = 0.85 - 1.15$, $n = 1.77 - 2.4$ for 3C345.

The projection of the opening half-angle $\phi_{ob} = \phi/\sin\theta$ is a measurable quantity. But this kind of the information is available only in a few sources. To derive the parameters of the inhomogeneous jet, we have to make some simplified assumptions. Blandford and Königl (1979) suggested $\phi \leq 1/\gamma$. Some authors (Hutler and Mufson 1986, and Mufson et al. 1988) adopted the assumption $\phi = 1/\gamma$ in their application of this model. Marscher (1987) argues that $\tan\phi = (\sqrt{3}\gamma)^{-1}$ for a free jet.

In our calculation, we assume $\alpha = 0.75$, $m = 1$, $n = 2$ and the opening half-angle $\phi = 1/\gamma$ in

Model A and $\alpha = 0.6$, $m = 1.5$, $n = 1.4$ and $\phi = 1/\gamma$ in Model B. The four independent variables n_1, B_1, β, and θ can be derived from Equations (2)−(4) and Königl's Equation (13) (Königl 1981). Thus, we obtain simultaneously the values of Lorentz factor γ, viewing angle θ, and Doppler factor δ.

Equation (1) of Ghisellini et al. (1993),

$$\delta = f(\alpha) F_m \left[\frac{\ln(\nu_b/\nu_m)}{F_x \theta_d^{6+4\alpha} \nu_x \nu_m^{5+3\alpha}} \right]^{1/(4+2\alpha)} (1+z), \tag{8}$$

is used to compare the results of the homogeneous sphere model, where F_x is the X-ray at frequency ν_x, F_m, θ_d are the radio flux density and the angular size of the core at the turnover frequency ν_m. The VLBI observing frequency is assumed to be ν_m. We assign the homogeneous sphere model with $\alpha = 0.75$ as Model C . The values $H_0 = 75\ kms^{-1}Mpc^{-1}$ and $q_0 = 0.5$ are used throughout this work.

3. SAMPLE

We have searched the literature for objects which have relevant data, such as the radio flux density and the size of the core, the proper motion and X-ray flux density . The VLBI core and X-ray data have been presented by Ghisellini et al. (1993), while Vermeulon and Cohen (1994) have compiled the proper motion data. The selection criterion of our sample is that all sources have VLBI measurements of proper motion of outflowing plasma. A total of 52 sources were chosen after a careful literature search, in which 17 sources are detected EGRET γ-ray sources. The observational data for the sample are presented in Table 1, which gives the redshift (z), VLBI core size (θ_d), and radio flux (S_c) at the frequency ν_s, 1 keV X-ray flux density (S_x) and the proper motion (μ_{app}) with necessary references. The redshift of 0716+714 is not available, and a value of 0.3 is assumed in the calculation. For 1823+568, only the 2 keV X-ray flux density is given, and the 1 keV X-ray flux density was derived by assuming a spectral index of 1.30, which is the average value for BL Lacs. We assume that all the observed X-ray flux density is attributed to the SSC emission in the derivation, which will result in some uncertainties. Also the X-ray observations are not contemporaneous with the VLBI observations, and this will introduce some uncertainties too. However our calculations show that the value of X-ray flux density is not sensitive to the derived parameters. Another uncertainty of data is the proper motion. We assume the fastest one when there are more than one moving components. Even though it is not quite certain that the observed proper motion could represent the real information of the core, we think that the observed proper motion is a good approximation.

4. RESULTS

Using the method described in § 2 the jets' parameters of all the sources in our sample are derived. The results are shown in Tables 2A and 2B for above mentioned models A and B, respectively. We note that there is no big difference between the results from these two models, so we will discuss only model A when comparing to the homogeneous model (model C).

4.1. *The distribution of Doppler factor and Lorentz factor*

In Figure 1 we show the distribution of the derived Doppler factor δ for the 17 EGRET sources and the 45 remaining sources in our sample. The EGRET sources have higher values of δ, except three BL Lacs: 0716+714, 1101+384(Mrk421), and 1219+285. The distribution of the Lorentz factor γ are plotted in Figure 2. Similarly, it is found that the EGRET sources have relatively high values of γ. From Figures 1 and 2 we note that there are some objects with high values of δ or γ have not been measured γ-ray radiation by EGRET. Compared with the other EGRET sources, three BL Lacs 0716+714, Mrk421, and 1219+285 have relatively low values of both δ and γ. The BL Lac object Mrk421 is a special one because of its detection as an TeV source as well as EGRET source. The redshift of object 0716+714 is not available, with an assumed 0.3, which would probably increase the uncertainty of its derived parameters. These three objects show interesting characters.

Figure 3a is the plot of Lorentz factors γ for all the objects in our sample with $\delta > \delta_c$, where $\delta_c = 4.5$ for model A. The 14 EGRET sources show large values of Lorentz factor γ with $\gamma \geq 10$. Similar phenomena are shown for model B, where $\delta_c = 3.5$. Almost all of the remaining objects with $\delta > \delta_c$ show relatively lower Lorentz factors γ except the source 1308+326. Figure 3b is the results of model C which has $\delta_c = 2.5$.

The statistical information of the Doppler factor δ, Lorentz factor γ, and the viewing angle θ for the different classes of the sources in our sample are listed in Table 3. In Figure 4 the Lorentz factor γ vs. the viewing angle θ for all sources is depicted.

4.2. *The distribution of turnover frequency*

In our model the observed turnover frequency ν_{sM} of the radio continuum could be naturally derived. If there are enough dedicated measurements on the turnover frequency, it will offer an effective examination on our model. Estimates of the synchrotron self-absorption frequency for some sources (Bloom et al., 1994; Reich et al., 1993) seem to be compatible with our results. We depict the distribution of the turnover frequency in the sources' rest frame $(1 + z)\nu_{sM}$ in Figure 5. The EGRET sources have relatively higher turnover frequencies measured in the sources' rest frame compared with the other sources in our sample. This could be the natural conclusion drawn

from the fact that the EGRET sources have high values of Doppler factor (§ 4.1). No obvious difference is found in the intrinsic turnover frequencies ($\nu_{sM}(1+z)/\delta$) between the EGRET and the rest of the sources in our sample.

4.3. *Correlation of brightness temperature $(1+z)T_b$ in the source's rest frame with Doppler factor δ*

In Figure 6a and 6b we plot the brightness temperatures in the sources' rest frame $(1+z)T_b$ vs. the Doppler factor δ derived from model A and C, respectively. The observed 22GHz brightness temperatures T_b are taken from Moellenbrock et al. (1996). The total number of sources is 31, within which 13 sources only have low limits on the brightness temperature. There are significant correlations (at 99.9% for both model A and B) between the brightness temperature in the source's rest frame and the Doppler factor derived from model A and B, respectively. In calculating the correlation, the source 0016+731 is not included, the brightness temperature of this source is only given a lower limit. The best correlation for the data derived from model A and B are: $\log(1+z)T_b = 10.98 + 0.84\log\delta$ and $\log(1+z)T_b = 11.00 + 0.93\log\delta$, respectively. A less significant correlation is found for model C: $\log(1+z)T_b = 11.22 + 0.45\log\delta$ (a correlation coefficient $r = 0.39$, at 98% level). The correlation derived from our model seems to agree with the prediction: $(1+z)T_b \propto \delta$.

The correlation between the values of the Doppler factor δ derived from models A and C is also examined as shown in Figure 7. A good correlation is found, which means the statistical behavior of the Doppler factor derived from homogeneous sphere model has no significant difference from our model. Nonetheless, the values of the Lorentz factor γ derived in the homogeneous sphere model for some sources would be as high as several hundred, which is mainly due to extremely low estimate on the Doppler factor for these sources (Ghisellini et al. 1993). The proper motion data are not taken into account in the derivation of the Doppler factor δ in homogeneous sphere model. In our model, the proper motion information is used in the derivation of both the Doppler factor δ and Lorentz factor γ. We suggest that the homogeneous sphere model could be used especially for the sources without the data of proper motion.

4.4. *Correlation of the relative γ-ray luminosity with the Doppler factor δ*

Recently, about fifty AGN have been detected high energy γ-ray emission by EGRET(von Montigny et al., 1995; Thompson et al. 1995). 17 EGRET sources are listed in our sample. We present the correlation of the relative γ-ray luminosity L_γ with the Doppler factor δ in Figure 8a. The relative γ-ray luminosity L_γ is simply defined by $L_\gamma = d_L^2 F$, where d_L is the luminosity distance, F is the maximum photon flux in γ-ray range taken from von Montigny et al. (1995) and Thompson et al. (1995). The best correlation for the data derived from models A and B

are: $\log L_\gamma = -1.80 + 2.45 \log \delta$ (at 99.9% level) and $\log L_\gamma = -1.59 + 2.52 \log \delta$ (at 99.9% level), respectively. We find the correlation, $\log L_\gamma = -0.94 + 1.58 \log \delta$ (at 99.9% level), for model C, which is plotted in Figure 8b.

5. DISCUSSION

We summarize the main results obtained in the previous sections as follows:

1. The values of the Doppler factor δ of the EGRET sources are higher than those of the non EGRET sources in our sample except three BL Lacs: Mrk421, 0716+714, and 1219+285, though some sources other than the EGRET sources also have high δ. The values of Lorentz factor γ of the EGRET sources show similar behavior.

2. The EGRET sources except the three BL Lacs, have both large values of the Lorentz factor γ (≥ 10) and δ ($\delta \geq \delta_c$, $\delta_c = 4.5, 3.5$, for models A and B, respectively), which seems to be the significant difference between the EGRET and the remaining sources in the sample.

3. The derived turnover frequency $(1+z)\nu_{sM}$ measured in the sources' rest frame are higher for the EGRET sources than the rest sources in the sample, though there still some sources other than the EGRET sources have high turnover frequencies.

4. The BL Lacs have a similar mean Lorentz factor γ with the core-dominated quasars, but the mean viewing angle θ of the BL Lacs is slightly larger than that of the core-dominated quasars. The lobe-dominated quasars have a large mean viewing angle $\sim 40^\circ$, while for the core-dominated quasars it is $\sim 10^\circ$.

5. There are significant correlations between the brightness temperature in the sources' rest frame $(1+z)T_b$ and the Doppler factor δ for both Models A and B. No similar significant correlation is found for Model C.

6. The significant correlations of the relative γ-ray luminosity L_γ are found with the Doppler factor δ for both model A and B.

There are 17 EGRET sources included in our sample. Except three BL Lacs, all of the remaining 14 EGRET sources show high value of δ and γ. The mean viewing angle of 14 EGRET sources are 4.9° and 5.7° for Model A and B, respectively. We have not seen any difference on the intrinsic physical properties between these two types of sources from our statistical results. These suggest that the γ-ray emissions from the AGN are mainly due to the beaming effects. Only the sources with high Doppler factor δ, which are strongly beamed to us, are detected at γ-ray energies. For the synchrotron self-Compton model of γ-ray production, the Doppler factor δ rather than Lorentz factor γ of the bulk motion of the jet plays crucial roles on the observed γ-ray flux. Sikora, Begelman & Rees (1993, 1994) have proposed that the γ-ray emission originates in a jet as a product of inverse Compton scattering of relativistic electrons and seed photons

produced externally to the jet. Moving in a homogeneous photon 'bath' (produced by material scattering photons from the disk, or by the broad-line region), the jet would 'see' this radiation energy density amplified by a factor γ^2. Therefore in this model the Lorentz factor γ together with Doppler factor δ determine the γ-ray radiation. The fact that some sources with high Doppler factor δ and low Lorentz factor γ have not been detected the γ-ray emission might imply that the seed photons are from somewhere outside the jet, if the γ-ray detected by EGRET is due to the inverse Compton scattering of lower energy photons up to γ-ray energies by beamed relativistic electrons. Thus, the sources with low Lorentz factor cannot produce sufficient γ-rays through inverse Compton scattering of the external soft photons.

The source 1308+326 has both high δ and γ similar to the EGRET sources in the sample but it is non EGRET source. This might be due to the measurements on the value of proper motion. The overestimation on the proper motion of the source would lead to the overestimation of its δ and γ . The further VLBI measurement on the proper motion of this object is necessary. The other possibility is that the object is a γ-ray source just in the quiescent state and therefore has not been detected by EGRET.

We cannot see significant differences on the mean values of δ, γ, and θ of the BL Lacs from that of the all sources in the sample (Table 3). The mean value of the Lorentz factor γ of the BL Lacs is similar to that of the core-dominated quasars and the mean viewing angle of BL Lacs is slightly larger than that of the core-dominated quasars. The mean values of Doppler factor show that the core-dominated quasars are more beamed than the BL Lacs. The results obtained here seem not to agree with the previous suggestion that the viewing angle of BL Lacs are smaller. Three BL Lacs Mrk421, 0716+714 and 1210+285 are quite special, which have relatively low Lorentz and Doppler factors, and large viewing angle, but are detected at γ-ray energies. One possible reason might be that the BL Lac objects have a different radiation mechanism from the other AGNs. Urry (1994) suggested that the X-ray emission from the BL Lacs are due to the synchrotron radiation instead of the synchrotron self-Compton radiation. Thus, there may be some problems in using a single model to describe all AGNs.

It is shown in Table 3 that the core-dominated and lobe-dominated quasars have rather different mean values of viewing angle. These two types quasars may be the same phenomenon, but seen at different viewing angles, which is consistent with the previous results (Ghisellini et al. 1993) and the unified scheme.

The correlation between the brightness temperature in the source's rest frame $(1 + z)T_b$ and the Doppler factor δ derived in our model suggest that the derived values of beaming parameters are a good approximation. As a comparison the correlation is less significant for the homogeneous sphere model. However, the homogeneous sphere model is useful to estimate the Doppler factor, especially for the objects without proper motion data, since the derived Doppler factor from the homogeneous sphere model is in general compatible with that from our inhomogeneous jet model (see Figure 7). The correlation of the relative γ-ray luminosity L_γ with the Doppler factor δ

presented in Figure 8 strongly suggests that the γ-ray emission from the AGN are beamed, though the detailed mechanism for γ-ray emission is still not clear.

Two sets of parameters α, m, and n are adopted in the model calculations and we adopted the same values of these parameters for all sources in one model calculation. In practice, the sources may have different values of parameters α, m, and n, and, in principle, these parameters could be constrained by the observable quantities α_{S1}, α_{C2}, and k_m. Unfortunately, the information is only found for a few cases through multi-frequencies VLBI observations. Further high resolution multi-frequencies VLBI observations would be helpful to improve our model calculations.

We thank the referee for his helpful comments on the manuscript. The support from Pandeng Plan is gratefully acknowledged. XC thanks the support from Shanghai Observatory, China Post-Doctoral Foundation, and NSFC.

REFERENCES

Biretta, J. A., Zhou, F., Owen, F. N., 1995, ApJ, 447, 582

Blandford, R. D., Königl, A., 1979, ApJ, 232, 34

Bloom, S. D., Marscher, A. P., Gear, W.K. et al., 1994, AJ, 108, 398

Brunner, H., Lamer G., Worrall, D. M., Staubert R., 1994, A&A, 287, 436

Chu, H. S., Baath, L. B., Rantakyrö. F. T., Zhang, F. J., & Nicholson, G., 1996, A&A, 307, 15

Doeleman, S., Rogers, A. E. E., & Moran, J. M., 1994, in Proc. 2nd EVN/JIVE Symposium, Torun, ed. Kus, A. J., Schilizzi, R. T., Borkowski, K. M., & Gurvits, L. I., 39

Gabuzda, D. C., Cawthorne, T. V., Roberts, D. H., & Wardle, J. F. C., 1992, ApJ, 388, 40

Gabuzda, D. C., Kollgaard, R. I., Roberts, D. H., 1993, ApJ, 410, 39

Gabuzda, D. C., Mullan, C. M., Cawthorne, T. V., Wardle, J. F. C., & Roberts, D. H., 1994, ApJ, 435, 140

Ghisellini, G., Padovani, P., Celotti, A., & Maraschi, L., 1993, ApJ, 407, 65

Güijosa, A., & Daly, R. A., 1996, ApJ, 461, 600

Hough, D. H., 1994, in Compact Extragalactic Radio Sources, New Mexico, ed. Zensus, J. A., & Kellermann, K. I., 169

Hutter, D. J., & Mufson, S. L., 1986, ApJ, 301, 50

Kellerman, K. I., Shaffer, D. B., Purcell, G. H., et al., 1977, ApJ, 211, 658

Kollgaard, R. I., Wardle, J. F. C., Roberts, D. H., 1990, AJ, 100, 1057

Königl, A., 1981, ApJ, 243, 700

Krichbaum, T. P., Standke, K. J., Witzel, A. et al., 1994, in Proc. 2nd EVN/JIVE Symposium, Torun, ed.

Kus, A. J., Schilizzi, R. T., Borkowski, K. M., & Gurvits, L. I., 47

Ku, W. H. M., Helfand, D. J., Lucy, L. B., 1980, Nature, 288, 323

Lamer, G., Brunner, H., Staubert, R., 1996, A&A, 311, 384

Lawrence, C. R., Readhead, A. C. S., Linfield, R. P., et al., 1985, ApJ, 296, 458

Linfield, R. P., Levy, G. S., Edward C. D. et al., 1990, ApJ, 358, 350

Linfield, R. P., Levy, G. S., Ulvestad, J. S., et al., 1989, ApJ, 336, 1112

Moellenbrock, G. A., Fujisawa, R. A., Preston, R. A. et al., 1996, AJ, 111, 2174

Mufson, S. L., Hutter, D. J., Kondo, Y., 1989, in Lecture Notes in Physics, Vol.334, BL Lac Objects, ed. Maraschi, L., Maccacaro, T., Ulrich, M.-H., (Berlin: Springer), 341

Mutel, R. L., 1990, In Parsec-Scale Radio Jets, ed. Zensus, J.A., and Pearson, T. J. (Cambridge Univ. Press), 98

Padovani, P., 1992, A&A, 256, 399

Padovani, P., Giommi, P., Fiore, F., 1997, MNRAS, 284, 569

Padovani, P., Urry, C. M., 1992, ApJ, 387, 449

Pearson, T. J., Readhead, A. C. S., 1988, ApJ, 328, 114

Polatidis, A. G., et al., 1995, ApJS, 98, 1

Porcas, R. W., 1987, in Superluminal Radio Sources, ed. Zensus, A., & Pearson, T. (Cambridge Univ. Press), 12

Rantakyrö, F. T., Baath, L. B., Dallacasa, D., Jones, D. L., Wehrle, A. E., 1996, A&A, 310, 66

Readhead, A. C. S., 1994, ApJ, 426, 51

Reich, W., Steppe, H., Schlickeiser, R. et al., 1993, A&A, 273, 65

Shen, Z. Q., 1996, Ph. D. thesis, Shanghai Observatory

Sikora, M., Begelman, M. C., Rees, M. J., 1993, in AIP Proc. 280, Compton Gamma-ray Observatory, eds Friedlander, M., Geherels N., Macomb, D. J., New York, 598

Sikora, M., Begelman, M. C., Rees, M. J., 1994, ApJ, 421, 153

Taylor, G. B., Vermeulen R. C., Pearson T. J., Readhead, A. C. S., Henstock D. R., Browne, I. W. A., & Wilkinson, P. N., 1995, ApJS, 95, 345

Thakkar, D. D., Xu, W., Readhead, A. C. S., Pearson, T. J., Tayler, G. B., Vermeulen, R. C., Polatidis, A. G., & Wilkinson, P. N., 1995, ApJS, 98, 33

Thompson, D. J., Bertsch, D. L., Dingus, B. L., et al., 1995, ApJS, 101, 259

Unwin, S. C., Wehrle, A. E., Urry, C. M., Gilmore, D. M., Barton, E. J., Kierulf, B. C., Zensus, J. A., & Rabaca, C. R., 1994, ApJ, 432, 103

Urry, C. M., 1994, in Frontiers of Space and Ground-based Astronomy, ed. Wamsteker, W., Longair, M. S., Kondo, Y. (Netherlands: Kluwer), 335

Vermeulen, R. C., Bernstein, R. A., Hough, D. H., & Readhead, A. C. S., 1993, ApJ, 417, 541

Vermeulen, R. C., Cohen, M. H., 1994, ApJ, 430, 467

von Montigny, C., Bertsch, D. L., Chiang, J., et al., 1995, ApJ, 440, 525

Webb, J. R., Shrader, C. R., Balonek, T. J., et al., 1994, ApJ, 422, 570

Wilkes, B. J., Tananbaum H., Warral D. M., et al., 1994, ApJS, 92, 53

Zensus, J. A., 1989, in Lecture Notes in Physics, Vol. 334, BL Lac Objects, ed. Maraschi, L., Maccacaro, T., and Ulrich, M.-H. (Berlin:Springer), 3

Zhang, Y. F., Marscher, A. P., Aller, H. D., Aller, M. F., Teräsranta, H., & Valtaoja, E., 1994, ApJ, 432, 91

Fig. 1.— The distributions of the Doppler factor δ for the EGRET sources (solid) and the rest of the sources in the sample (dotted) derived from Models A (a) and C (b), respectively.

Fig. 2.— The distributions of the Lorentz factor γ for the EGRET sources (solid) and the rest of the sources in the sample (dotted) derived from Models A (a) and C (b), respectively.

Fig. 3.— The Lorentz factor γ for the sources with Doppler factor $\delta > \delta_c$ in the sample corresponding to Models A (a) and C (b), respectively. *Triangles*: EGRET sources; *circles*: the rest sources.

Fig. 4.— The Lorentz factor γ vs. the viewing angle θ for all sources in the sample derived from Model A. *Triangles*: EGRET sources; *circles*: the rest sources. The dashed line represents $\gamma = 1/\sin\theta$.

Fig. 5.— The distributions of the turnover frequency $\nu_{sM}(1+z)$ in the source's rest frame for the EGRET sources (solid) and the rest sources in the sample (dotted) derived from Models A (a) and C (b), respectively.

Fig. 6.— The intrinsic brightness temperature in the source's rest frame vs. the Doppler factor δ derived from Models A (a) and C (b), respectively. Arrow symbols indicate the low limits on the brightness temperature.

Fig. 7.— The Doppler factor δ derived from Model A vs. that from Model C. *Triangles*: EGRET sources; *circles*: the remaining of sources.

Fig. 8.— The relative γ-ray luminosity vs. the Doppler factor δ derived from Models A (a) and C (b), respectively.

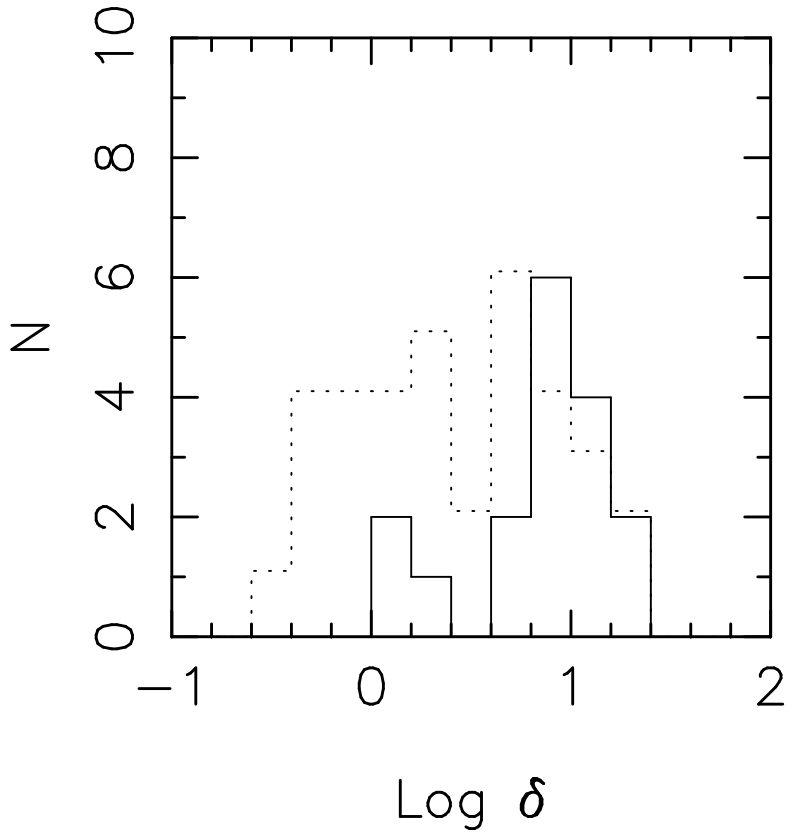

fig. 1a.

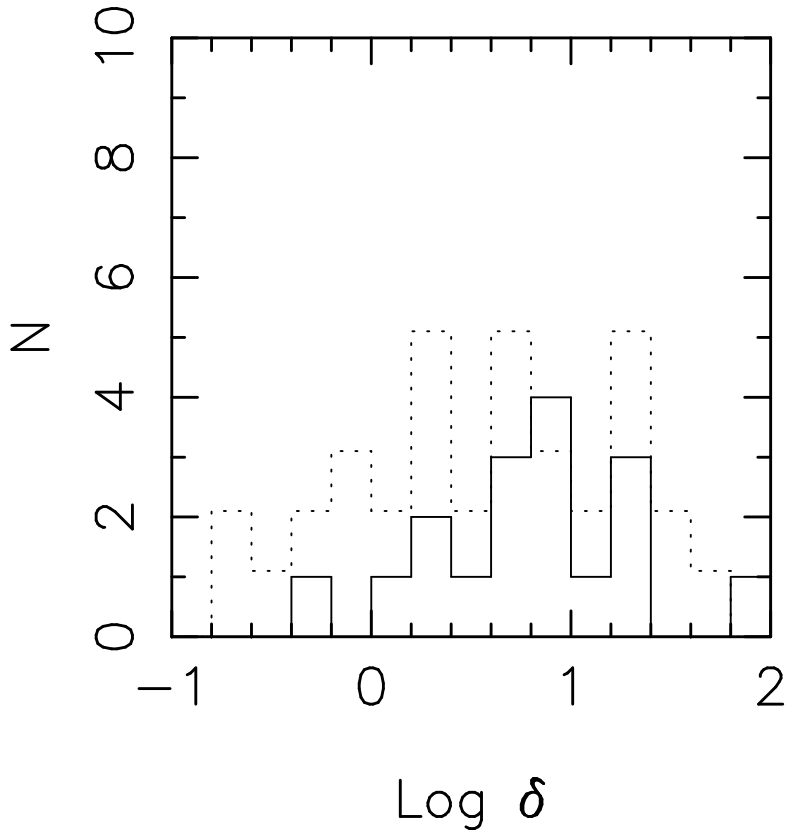

fig. 1b.

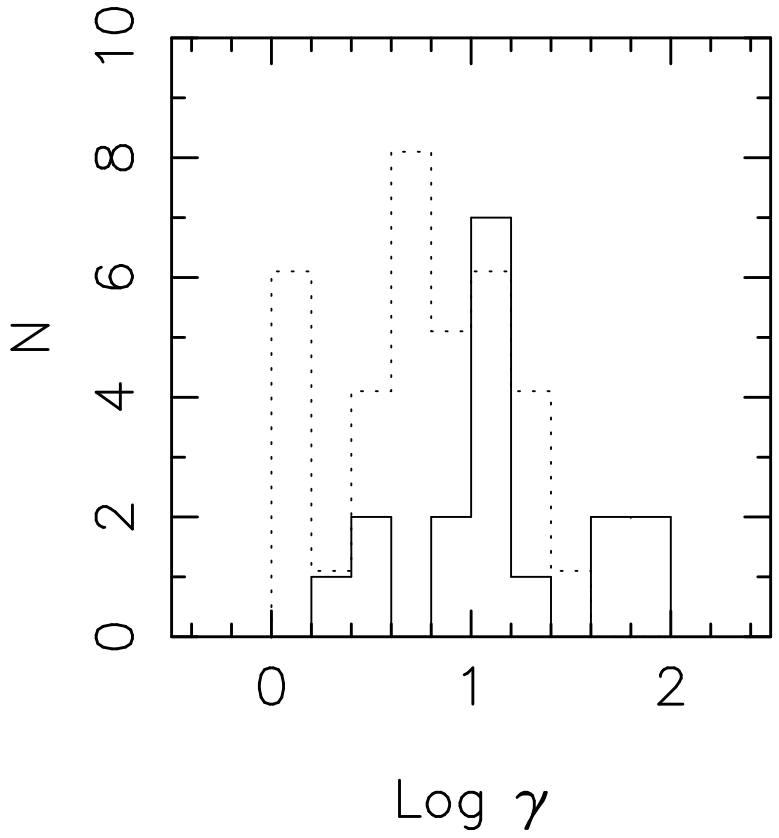

fig. 2a

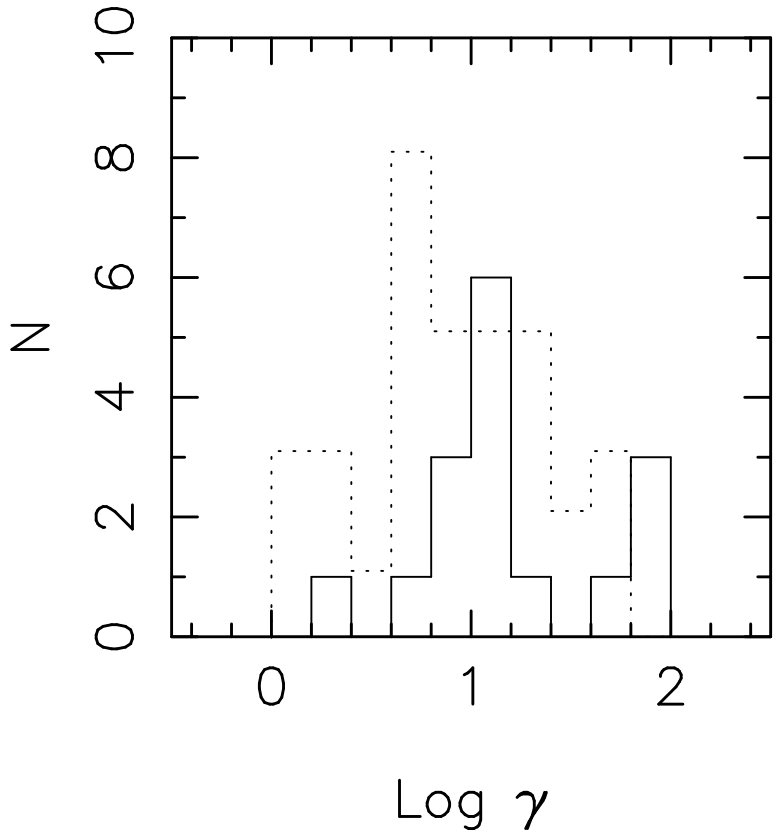

fig. 2b.

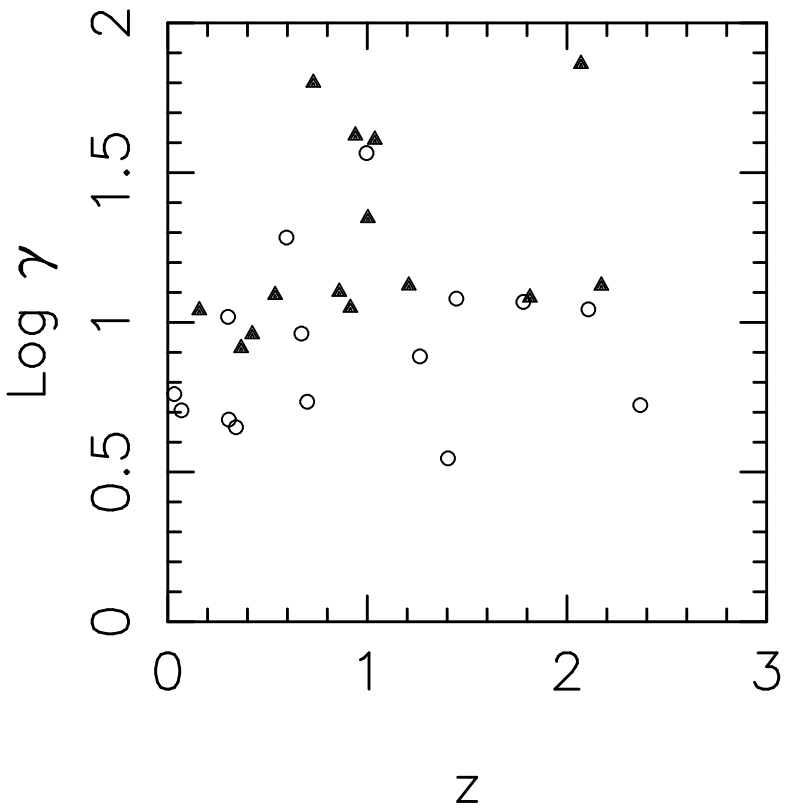

fig. 3a.

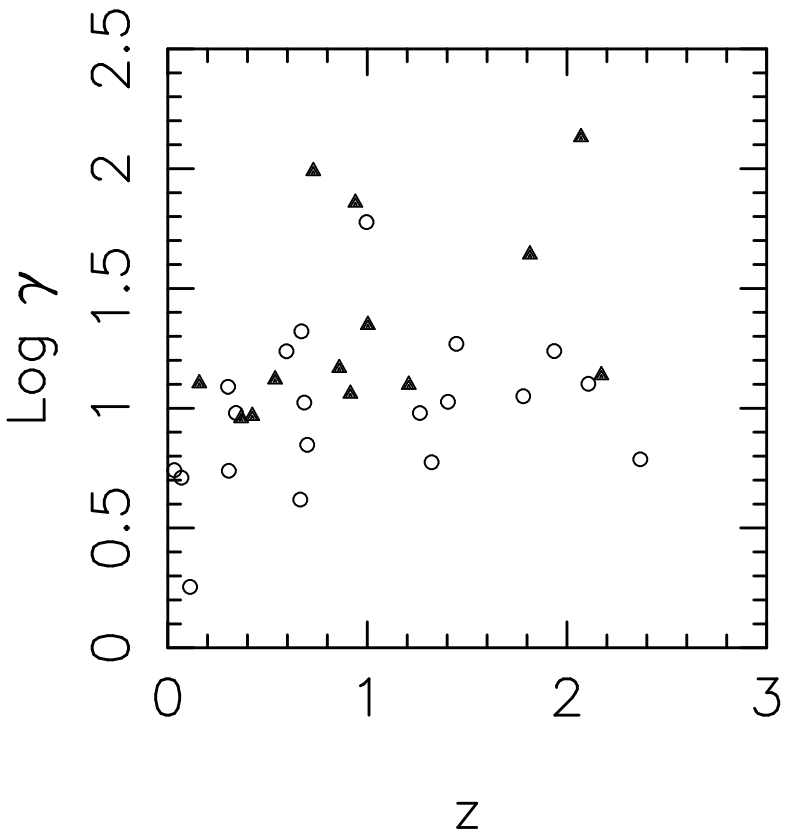

fig. 3b.

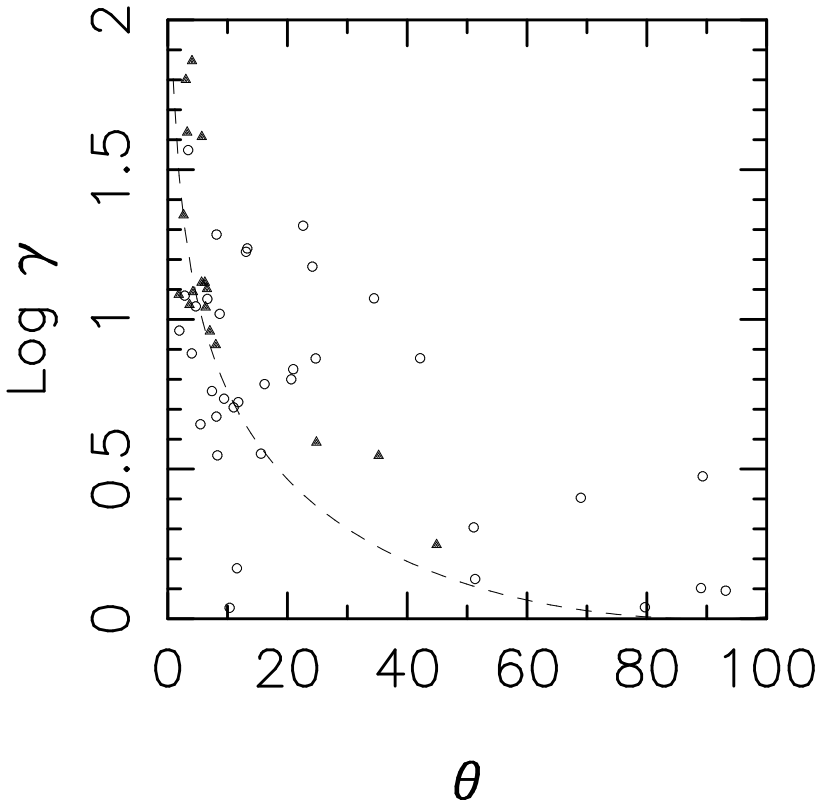

fig. 4.

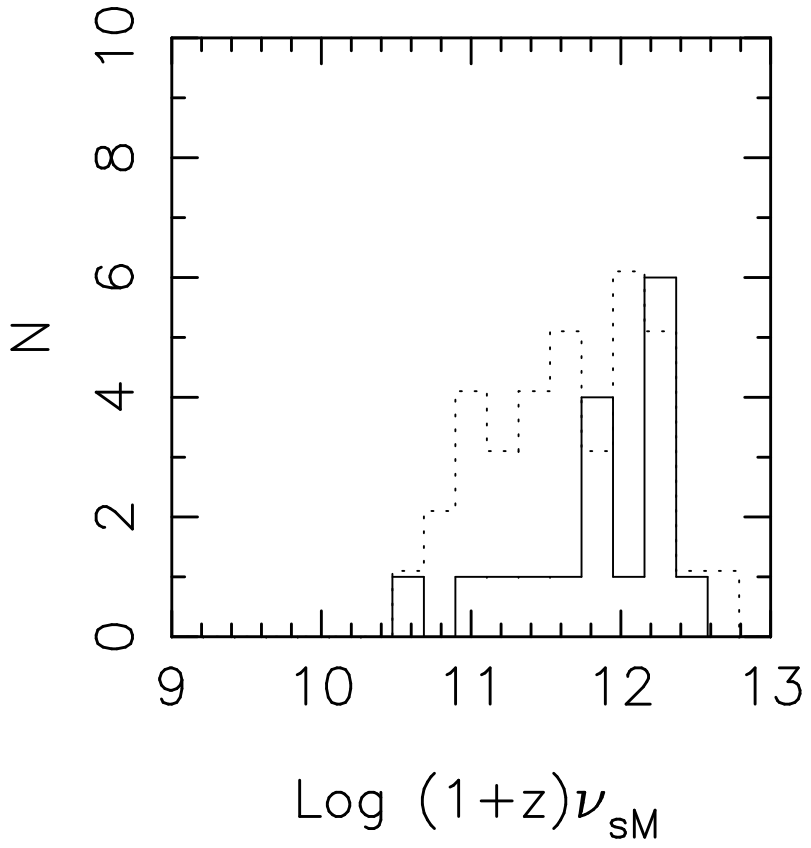

fig. 5a

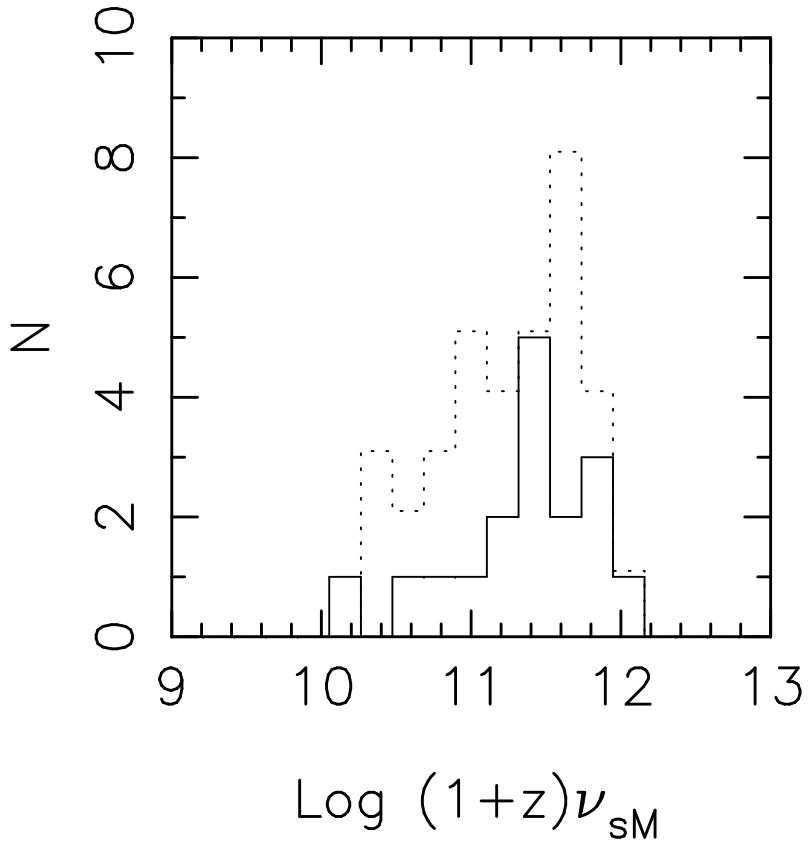

fig. 5b.

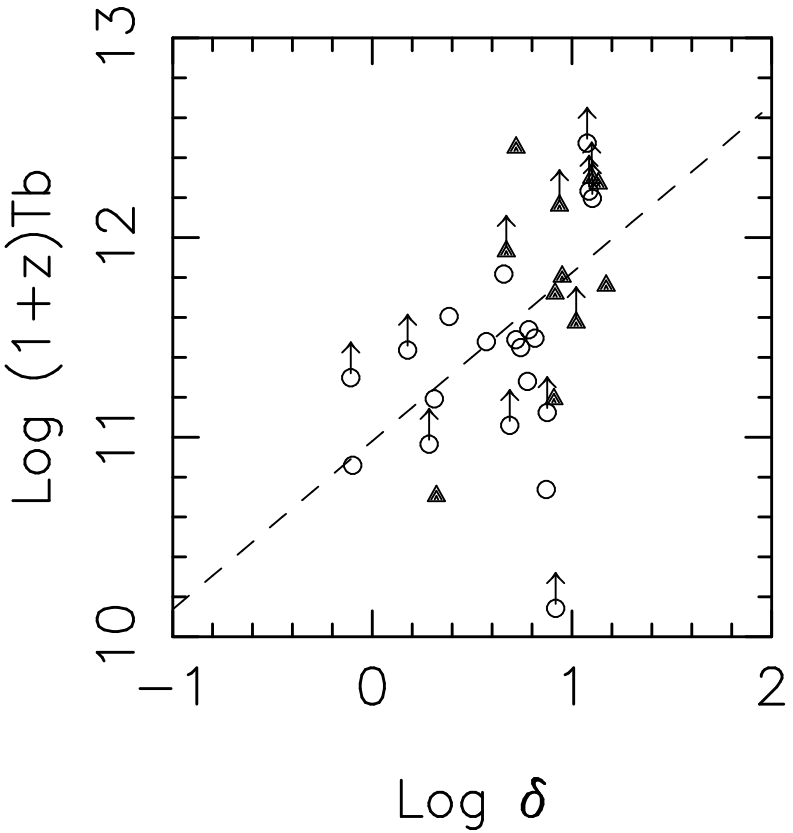

fig. 6a.

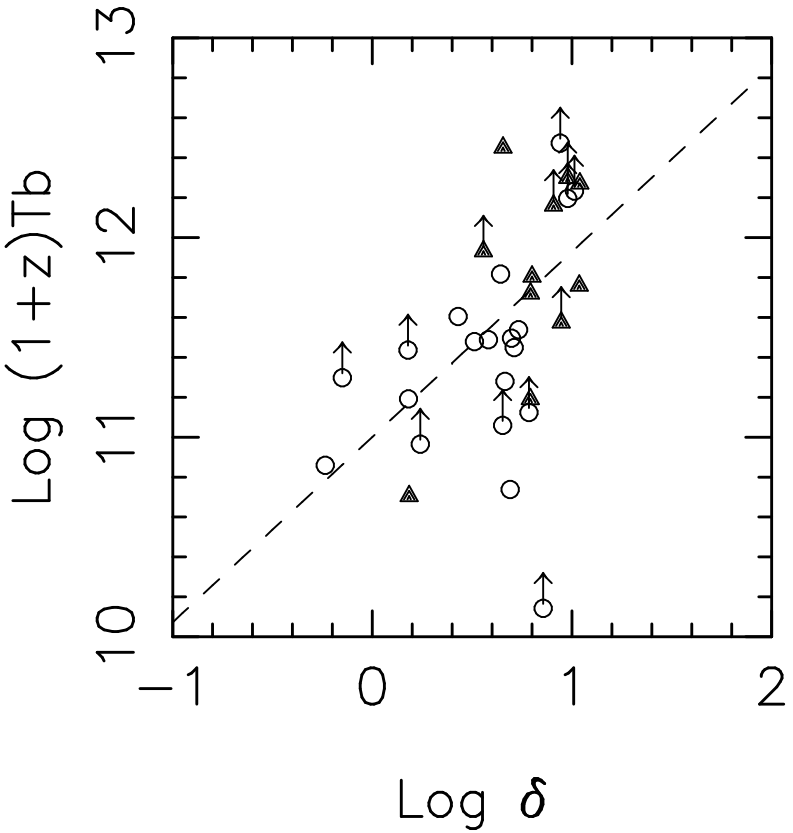

fig. 6b.

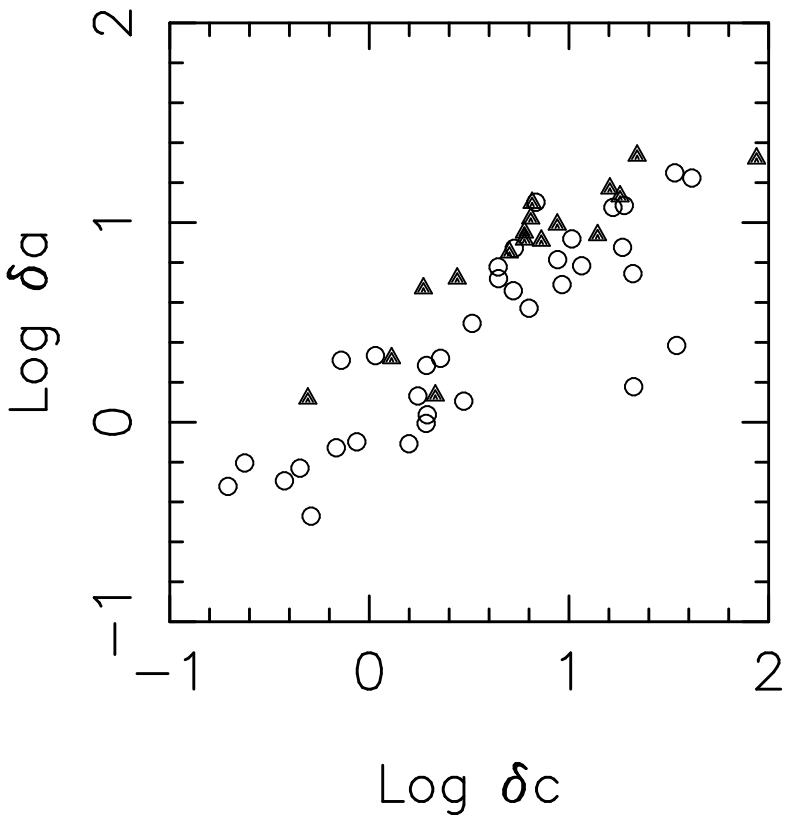

fig. 7.

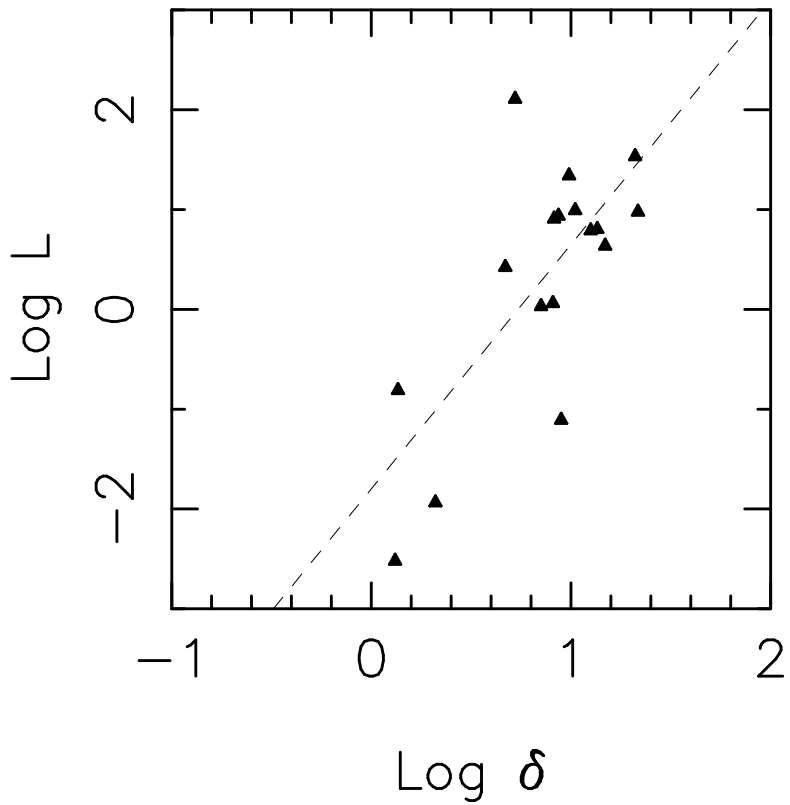

fig. 8a

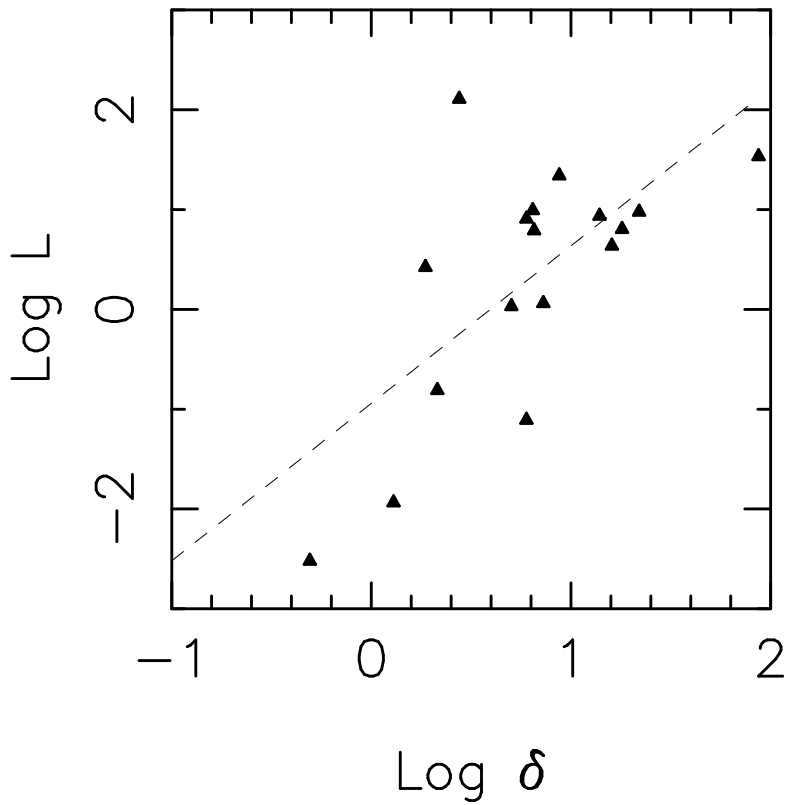

fig. 8b.

TABLE 1

DATA OF VLBI AND X-RAY

Source	Class.	z	θ_d(mas)	$S_c(\nu_s)$(Jy)	ν_s(GHz)	Ref.	$S_X(\mu$Jy)	Ref.	μ_{app}(mas.yr^{-1})	Ref.
0016+731	Qc	1.781	0.46	1.58	5.0	(1)	0.12	(1)	0.22	(2)
0106+013	Qc	2.107	0.40	2.30	5.0	(1)	0.22	(1)	0.20	(2)
0133+207	Ql	0.425	0.22	0.082	10.7	(3)	0.753	(4)	0.24	(2)
0153+744	Qc	2.338	0.59	0.64	5.0	(1)	1.00	(1)	0.08	(2)
0208−512†	Q	1.003	0.35	2.77	5.0	(5)	0.08	(5)	0.60	(5)
0212+735	Qc	2.367	0.47	1.36	5.0	(1)	0.23	(1)	0.09	(2)
0234+285†	Q	1.207	0.1	1.70	22.3	(1)	0.15	(1)	0.3	(2)
0235+164†	BL	0.940	0.50	1.75	5.0	(1)	0.17	(1)	0.84	(6)
0316+413	G	0.017	0.30	6.0	22.2	(1)	18.0	(1)	0.54	(2)
0333+321	Qc	1.263	0.33	1.60	3.2	(1)	1.6	(1)	0.15	(2)
0415+379	G	0.0485	0.13	2.9	86.2	(7)	3.283	(4)	1.54	(2)
0420−014†	Qc	0.915	0.72	3.43	2.3	(1)	0.52	(1)	0.30	(8)
0430+052	G	0.033	0.40	3.90	5.0	(1)	10.0	(1)	2.66	(2)
0454+844	BL	0.112	0.55	1.3	5.0	(1)	0.05	(1)	0.14	(2)
0528+134†	Q	2.070	0.17	0.88	22.2	(9)	1.59	(9)	0.5	(9)
0615+820	Qc	0.710	0.50	0.61	5.0	(1)	0.20	(1)	0.05	(2)
0710+439	Qp	0.518	0.96	0.63	5.0	(1)	0.55	(1)	0.04	(10)
0716+714†	BL	0.30	0.35	0.50	5.0	(1)	0.22	(1)	0.09	(2)
0735+178†	BL	0.424	0.30	1.29	5.0	(1)	0.32	(1)	0.44	(2)
0836+710†	Qc	2.172	0.34	1.05	5.0	(1)	1.0	(1)	0.23	(2)
0850+581	Qc	1.322	0.48	0.94	5.0	(1)	0.97	(1)	0.12	(2)
0851+202	BL	0.306	0.30	2.30	5.0	(1)	1.70	(1)	0.27	(2)
0906+430	Qcl	0.670	0.104	0.875	5.0	(1)	0.09	(1)	0.18	(2)
0917+624	Q	1.446	0.115	1.22	8.4	(11)	0.12	(11)	0.23	(11)
0923+392	Qc	0.699	0.69	6.90	5.0	(1)	0.37	(1)	0.18	(2)
0954+658†	BL	0.368	0.19	0.477	5.0	(18)	0.5	(1)	0.44	(19)
1040+123	Qcl	1.029	0.33	0.59	10.7	(1)	0.121	(1)	0.11	(2)
1101+384†	BL	0.031	0.30	0.24	5.0	(1)	14.0	(1)	1.33	(2)
1150+812	Qc	1.250	0.50	0.46	5.0	(1)	0.20	(1)	0.11	(2)
1156+295†	Q	0.729	0.123	1.40	22.2	(1)	0.15	(1)	1.15	(2)
1219+285†	BL	0.102	0.20	0.159	5.0	(19)	0.42	(1)	0.55	(19)
1226+023†	Qc	0.158	0.14	3.49	15.0	(1)	21	(1)	1.20	(2)
1228+127	G	0.0032	0.70	1.0	5.0	(1)	0.68	(1)	3.07	(12)
1253−055†	Qc	0.538	0.14	4.84	15.0	(1)	1.4	(1)	0.50	(2)
1308+326	BL	0.996	0.50	1.97	5.0	(1)	0.30	(1)	0.75	(2)
1618+177	Ql	0.555	0.20	0.086	10.7	(1)	0.3	(1)	0.10	(2)
1633+382†	Qc	1.814	0.15	5.4	10.7	(13)	0.08	(14)	0.16	(10)
1637+826	G	0.023	0.20	0.67	10.7	(1)	0.30	(1)	0.3	(15)
1641+399	Qc	0.595	0.30	6.90	22.0	(1)	0.66	(1)	0.47	(2)
1721+343	Ql	0.2055	0.24	0.109	10.7	(1)	1.9	(1)	0.28	(2)
1749+701	BL	0.770	0.39	0.22	5.0	(1)	0.22	(1)	0.26	(2)
1803+784	BL	0.684	0.20	1.436	5.0	(1)	0.16	(1)	0.004	(2)
1807+698?	BL	0.051	0.79	0.95	5.0	(1)	0.60	(1)	2.6	(16)
1823+568	BL	0.664	0.35	1.132	5.0	(10)	0.2	(10)	0.12	(2)
1845+797	Ql	0.057	0.50	0.31	5.0	(1)	1.1	(1)	0.37	(17)
1928+738	Qc	0.302	0.49	2.11	5.0	(1)	0.55	(1)	0.60	(2)
2007+776	BL	0.342	0.19	1.361	5.0	(1)	0.11	(1)	0.18	(2)
2134+004	Qc	1.936	0.62	6.7	5.0	(1)	0.04	(1)	0.01	(15)

TABLE 1—*Continued*

Source	Class.	z	θ_d(mas)	$S_c(\nu_s)$(Jy)	ν_s(GHz)	Ref.	$S_X(\mu$Jy)	Ref.	μ_{app}(mas.yr^{-1})	Ref.
2200+420	BL	0.069	0.35	1.60	5.0	(1)	0.82	(1)	1.2	(2)
2223−052	Qc	1.404	0.10	1.98	15.0	(1)	1.1	(1)	0.06	(2)
2230+114†	Qp	1.037	0.50	0.54	5.0	(1)	0.34	(1)	0.5	(2)
2251+158†	Qc	0.859	0.30	0.90	5.0	(1)	0.56	(1)	0.35	(2)

† EGRET source; Q: quasar; Qc: core-dominated quasar; Ql: lobe-dominated quasar; Qp: Giga-Hertz peaked quasar; G: Galaxy.

REFERENCES.—(1) Ghisellini et al., 1993; (2) Vermeulen & Cohen, 1994; (3) Vermeulen et al., 1993; (4) Wilkes et al., 1994; (5) Shen, 1996; (6) Chu et al., 1996; (7) Doeleman et al., 1994; (8) Krichbaum et al., 1994; (9) Zhang et al., 1994; (10) Pearson and Readhead, 1988; (11) Rantakyrö et al., 1996; (12) Biretta, Zhou, & Owen, 1995; (13) Kellermann et al., 1977; (14) Ku, Helfand, & Lucy, 1980; (15) Zensus, 1989; (16) Mutel, 1990; (17) Porcas, 1987; (18) Gabuzda et al., 1992; (19) Gabuzda et al., 1994.

TABLE 2A

DERIVED JET PARAMETERS IN MODEL A

Source	Class.	θ(degree)	γ	δ	B_1(gauss)	n_1(cm^{-3})	ν_{sM}(GHz)
0016+731	Qc	6.6	11.7	8.3	3.85E−01	7.88E+05	2.3E+02
0106+013	Qc	4.7	11.1	12.2	3.63E−01	6.34E+04	2.6E+02
0133+207	Ql	22.6	20.5	0.6	1.64E−01	1.21E+06	2.8E+02
0153+744	Qc	20.6	6.3	2.1	1.95E−01	1.18E+06	1.0E+02
0208−512†	Q	2.6	22.3	21.7	5.07E−01	1.10E+04	7.9E+02
0212+735	Qc	11.8	5.3	4.9	2.33E−01	1.63E+05	1.4E+02
0234+285†	Q	6.2	13.3	8.7	3.63E−01	4.98E+04	3.7E+02
0235+164†	BL	3.3	42.1	12.6	6.79E−01	6.43E+04	8.0E+02
0316+413	G	93.2	1.2	0.8	1.10E−02	4.40E+03	2.2E+02
0333+321	Qc	4.0	7.7	11.9	1.44E−01	2.88E+04	7.8E+02
0415+379	G	24.1	15.0	0.7	1.58E−01	1.65E+05	2.6E+02
0420−014†	Qc	3.7	11.2	14.8	2.69E−01	1.81E+04	7.3E+02
0430+052	G	7.4	5.8	7.4	2.45E−02	3.52E+02	2.8E+03
0454+844	BL	51.3	1.4	1.3	4.14E−02	2.90E+03	7.7E+01
0528+134†	Q	4.1	73.0	5.2	9.11E−01	3.70E+06	3.4E+01
0615+820	Qc	51.1	2.0	1.1	8.76E−02	1.16E+05	5.9E+01
0710+439	Qp	89.3	3.0	0.3	1.45E−01	1.76E+06	3.0E+01
0716+714†	BL	44.9	1.8	1.4	4.33E−02	1.42E+04	1.3E+02
0735+178†	BL	7.0	9.1	8.1	1.41E−01	7.09E+03	7.9E+02
0836+710†	Qc	5.7	13.3	9.8	2.37E−01	1.31E+05	5.1E+02
0850+581	Qc	16.2	6.1	3.1	1.65E−01	2.39E+05	1.9E+02
0851+202	BL	8.1	4.7	6.5	7.93E−02	6.84E+03	7.7E+02
0906+430	Qcl	1.9	9.2	16.7	1.51E−01	2.06E+03	1.2E+03
0917+624	Q	2.8	12.0	17.7	2.53E−01	1.07E+04	7.0E+02
0923+392	Qc	9.4	5.4	6.1	2.85E−01	4.22E+04	1.8E+02
0954+658†	BL	8.0	8.2	7.1	7.41E−02	4.33E+03	1.3E+03
1040+123	Qcl	24.7	7.4	1.4	2.82E−01	5.04E+05	7.3E+01
1101+384†	BL	35.2	3.5	1.3	7.68E−03	1.58E+03	1.8E+03
1150+812	Qc	21.0	6.8	1.9	2.01E−01	2.98E+05	1.1E+02
1156+295†	Q	3.0	63.1	10.5	8.24E−01	8.66E+04	9.2E+02
1219+285†	BL	24.8	3.9	2.1	2.12E−02	1.40E+03	8.8E+02
1226+023†	Qc	6.3	11.0	8.9	7.18E−02	8.09E+03	2.4E+03
1228+127	G	89.0	1.3	0.8	3.79E−03	5.39E+01	4.1E+02
1253−055†	Qc	4.2	12.3	13.5	2.34E−01	1.64E+04	8.5E+02
1308+326	BL	3.4	36.7	12.6	5.96E−01	7.43E+04	8.2E+02
1618+177	Ql	42.1	7.4	0.5	1.11E−01	6.67E+05	1.0E+02
1633+382†	Qc	1.9	12.1	21.0	5.77E−01	2.27E+04	3.3E+02
1637+826	G	79.7	1.1	1.0	6.85E−03	4.50E+02	1.9E+02
1641+399	Qc	8.1	19.2	4.6	6.85E−01	3.14E+05	2.1E+02
1721+343	Ql	34.4	11.7	0.5	8.07E−02	4.97E+05	3.1E+02
1749+701	BL	13.1	16.8	2.2	2.22E−01	2.20E+05	3.2E+02
1803+784	BL	10.3	1.1	1.5	6.31E−02	8.08E+04	3.7E+01
1807+698	BL	13.3	17.2	2.0	9.82E−02	8.28E+03	8.1E+02
1823+568	BL	15.6	3.6	3.7	1.15E−01	2.05E+04	2.0E+02
1845+797	Ql	69.0	2.5	0.6	2.05E−02	9.33E+03	2.6E+02
1928+738	Qc	8.7	10.4	6.0	1.69E−01	1.37E+04	6.5E+02
2007+776	BL	5.5	4.5	7.5	1.01E−01	2.02E+03	5.3E+02
2134+004	Qc	11.6	1.5	2.4	3.12E−01	2.19E+05	1.4E+01

TABLE 2A—*Continued*

Source	Class.	θ(degree)	γ	δ	B_1(gauss)	n_1(cm^{-3})	ν_{sM}(GHz)
2200+420	BL	11.0	5.1	5.2	3.92E−02	6.40E+02	1.2E+03
2223−052	Qc	8.3	3.5	5.5	1.30E−01	6.89E+04	2.1E+02
2230+114†	Qp	5.7	40.7	4.7	5.10E−01	3.74E+05	6.4E+02
2251+158†	Qc	6.5	12.6	8.2	1.84E−01	3.12E+04	7.8E+02

† EGRET source.

TABLE 2B

DERIVED JET PARAMETERS IN MODEL A

Source	Class.	θ(degree)	γ	δ	B_1(gauss)	n_1(cm^{-3})	ν_{sM}(GHz)
0016+731	Qc	7.3	12.3	7.2	1.18E+00	7.98E+03	7.7E+01
0106+013	Qc	5.6	11.0	10.3	1.00E+00	7.04E+03	9.7E+01
0133+207	Ql	22.7	24.3	0.5	1.79E−01	4.86E+05	1.2E+02
0153+744	Qc	21.3	6.8	1.9	4.75E−01	1.15E+05	4.0E+01
0208−512†	Q	3.3	23.2	16.9	1.33E+00	2.17E+03	2.3E+02
0212+735	Qc	12.7	5.3	4.5	6.53E−01	1.22E+04	4.0E+01
0234+285†	Q	6.5	13.6	8.1	7.39E−01	6.03E+03	1.3E+02
0235+164†	BL	3.5	52.0	9.5	2.19E+00	1.51E+04	2.5E+02
0316+413	G	98.5	1.3	0.7	3.40E−03	4.76E+03	9.7E+01
0333+321	Qc	6.3	6.7	8.7	1.74E−01	1.05E+04	2.4E+02
0415+379	G	24.1	14.5	0.8	1.07E−01	3.97E+04	1.3E+02
0420−014†	Qc	5.3	10.6	10.9	5.61E−01	4.36E+03	2.0E+02
0430+052	G	11.7	5.5	4.9	5.63E−03	1.90E+03	9.4E+02
0454+844	BL	53.0	1.4	1.2	4.81E−02	5.27E+02	2.7E+01
0528+134†	Q	4.1	84.0	4.5	2.38E+00	5.09E+05	2.2E+02
0615+820	Qc	52.0	2.1	1.1	1.68E−01	1.05E+04	2.3E+01
0710+439	Qp	89.2	2.9	0.3	3.78E−01	7.76E+04	1.3E+01
0716+714†	BL	49.0	1.8	1.2	4.46E−02	4.07E+03	4.7E+01
0735+178†	BL	8.7	9.8	6.2	1.74E−01	3.68E+03	2.5E+02
0836+710†	Qc	6.6	14.6	7.6	4.43E−01	3.66E+04	1.7E+02
0850+581	Qc	17.4	6.6	2.7	3.34E−01	3.98E+04	7.1E+01
0851+202	BL	11.5	4.4	5.0	6.73E−02	3.91E+03	2.4E+02
0906+430	Qcl	3.2	7.4	12.6	1.39E−01	8.84E+02	3.3E+02
0917+624	Q	3.8	11.1	14.5	3.76E−01	2.55E+03	2.3E+02
0923+392	Qc	10.7	5.4	5.4	9.06E−01	3.21E+03	6.1E+01
0954+658†	BL	10.2	9.1	5.1	5.25E−02	5.78E+03	4.1E+02
1040+123	Qcl	24.7	7.3	1.4	7.20E−01	2.71E+04	3.0E+01
1101+384†	BL	39.3	4.8	0.9	1.21E−03	2.60E+04	6.6E+02
1150+812	Qc	21.5	7.3	1.7	4.71E−01	3.28E+04	4.3E+01
1156+295†	Q	3.1	73.3	8.8	1.92E+00	1.82E+04	3.5E+02
1219+285†	BL	28.4	4.6	1.5	7.22E−03	4.75+03	3.0E+02
1226+023†	Qc	7.9	12.4	6.3	3.63E−02	1.75E+04	1.0E+03
1228+127	G	102.6	1.5	0.6	5.90E−04	4.13E+02	1.3E+02
1253−055†	Qc	5.2	12.4	11.0	3.17E−01	5.30E+03	3.6E+02
1308+326	BL	3.7	45.1	9.5	1.81E+00	1.87E+04	2.6E+02
1618+177	Ql	42.3	7.9	0.5	1.26E−01	1.40E05	5.3E+01
1633+382†	Qc	2.2	11.3	18.9	1.92E+00	1.44E+03	1.1E+02
1637+826	G	95.0	1.1	0.9	1.86E−03	6.71E+02	7.3E+01
1641+399	Qc	8.2	19.8	4.4	2.27E+00	1.81E+04	9.5E+01
1721+343	Ql	34.7	14.0	0.4	5.87E−02	3.47E+05	1.4E+02
1749+701	BL	13.4	20.4	1.7	4.01E−01	6.71E+04	1.2E+02
1803+784	BL	10.2	1.1	1.5	1.82E−01	3.56E+03	1.5E+01
1807+698	BL	13.6	22.6	1.5	7.89E−02	1.20E+04	2.7E+02
1823+568	BL	17.9	3.6	3.2	1.90E−01	3.65E+03	6.8E+01
1845+797	Ql	71.4	3.0	0.5	9.39E−03	1.33E+04	9.7E+01
1928+738	Qc	9.8	12.0	4.6	2.58E−01	6.05E+03	2.1E+02
2007+776	BL	7.8	3.9	6.1	1.02E−01	6.92E+02	1.6E+02
2134+004	Qc	9.2	1.6	2.7	3.14E+00	1.83E+03	5.4E+00
2200+420	BL	14.6	5.3	3.8	1.72E−02	1.30E+03	3.7E+02
2223−052	Qc	9.4	3.4	5.1	1.97E−01	9.26E+03	9.1E+01
2230+114†	Qp	5.8	51.7	3.6	1.38E+00	9.79E+04	1.9E+02
2251+158†	Qc	7.6	14.4	6.2	2.77E−01	1.47E+04	2.5E+02

† EGRET source.

TABLE 3

MEAN VALUES

Source	N	Model	δ	θ	γ
All	52	A	6.2	20.5	12.3
		B	5.0	22.3	13.7
BL Lacs	15	A	5.0	17.0	10.6
		B	3.9	19.0	12.6
Qc*	26	A	8.8	9.8	14.2
		B	7.2	10.6	15.3
Ql	4	A	0.6	42.0	10.5
		B	0.5	42.8	12.3
G	5	A	2.1	58.7	4.9
		B	1.6	66.4	4.8

* Five Q are included in Qc.